Published in final edited form as:
*Proc SPIE*. 2010 February 23; 7625(2010): 762517–762518. doi:10.1117/12.844251.

# Accuracy validation for MRI-guided robotic prostate biopsy

**Helen Xu**[*,a], **Andras Lasso**[a], **Siddharth Vikal**[a], **Peter Guion**[b], **Axel Krieger**[c], **Aradhana Kaushal**[b], **Louis L. Whitcomb**[d], and **Gabor Fichtinger**[a,d]

[a]Queen's University, Kingston, Canada

[b]National Institutes of Health, Bethesda, USA

[c]Sentinelle Medical Inc., Toronto, Canada

[d]Johns Hopkins University, Baltimore, USA

## Abstract

We report a quantitative evaluation of the clinical accuracy of a MRI-guided robotic prostate biopsy system that has been in use for over five years at the U.S. National Cancer Institute. A two-step rigid volume registration using mutual information between the pre and post needle insertion images was performed. Contour overlays of the prostate before and after registration were used to validate the registration. A total of 20 biopsies from 5 patients were evaluated. The maximum registration error was 2 mm. The mean biopsy target displacement, needle placement error, and biopsy error was 5.4 mm, 2.2 mm, and 5.1 mm respectively. The results show that the pre-planned biopsy target did dislocate during the procedure and therefore causing biopsy errors.

### Keywords

Accuracy validation; image guided prostate biopsy; rigid volume registration; MRI

## 1. INTRODUCTION

Prostate cancer is the most common non-skin cancer among American men. It is estimated that in 2009, 192 280 men will be diagnosed with the disease and 27 360 men will die of it.[1] Currently, the prostate-specific antigen (PSA) test and the digital rectal exam (DRE) are two common screening methods for prostate cancer. The PSA concentration in blood estimates the likelihood of prostate cancer. In DRE, the physician examines the patient to determine whether abnormal lumps are present. When either test shows abnormal results, needle biopsy is often performed to determine if a tumor exists and whether it is benign or malign.[2]

Transrectal ultrasound (TRUS) is currently the standard imaging modality for guiding biopsy due to its low cost and ease-of-use.3 However, because of the poor image quality of ultrasound, TRUS only has a detection rate of 20–30%.4 Many studies have shown that this method misses the cancer in at least 20% of the cases.5–7 Magnetic resonance imaging (MRI) provides an alternative approach to the detection and diagnosis of prostate cancer. MRI has high spatial resolution, excellent soft tissue contrast, and volumetric imaging capabilities.[8]

[*]helen@cs.queensu.ca; phone 1 (613) 533-6000 Ext. 78234; Percutaneous Surgery Lab (Perk Lab), School of Computing, Queen's University, Kingston, Ontario, Canada, K7L 3N6.

Closed-bore MRI has strong magnetic fields and confined physical space; therefore such approach requires robotic assistance. Krieger *et al.* developed an MRI-guided robotic prostate biopsy system in 2003 (Figure 1).[2] Since then, over 200 biopsies were performed with this system by the U.S. National Cancer Institute (NCI). The robot guides a biopsy needle through the rectum into the targeted locations within the prostate to collect tissue samples. However, due to patient motion and organ dislocation during the procedure, the needle does not always reach the targeted region. This paper reports a quantitative evaluation of the clinical accuracy for this MRI-guided robotic biopsy system.

## 2. METHOD

### 2.1 Data acquisition

During the prostate biopsy procedure, the patient was first placed inside the MRI scanner in prone position to acquire a series of 2D high resolution T2 axial volumetric slices of the prostate. From this image volume, the clinicians selected the target point(s) for biopsy in RAS (Right, Anterior, Superior) coordinates and the robot was used to insert the needle. After the needle was in place, another set of 2D axial volumetric slices was taken to confirm needle placement. We used these pre and post needle insertion image sets to perform accuracy validation for the robotic prostate biopsy system.

### 2.2 Registration algorithm

A two-step 3D to 3D rigid registration using mutual information was performed using Insight Registration and Segmentation Toolkit (ITK) between the pre and post needle insertion image volumes (Figure 2). Rigid registration was used because we found the main prostate motion during the procedure to be rotation and translation.

In the first step of our implementation, the pre-insertion volume was used as the moving image, and the post insertion volume as the fixed image. The region of interest for both volumes was consisted of the rectum, prostate, and pubic bone. This step compensates for the prostate motion in coherence with the device and patient. The resulting image was then registered again with the original fixed image but using the prostate as the region of interest. This corrects for any residual decoupled prostate motion during the procedure. Movement in the superior and inferior direction was penalized because the first step should already correct for it.

### 2.3 Registration validation

This was a challenging step because the prostate does not show apparent anatomical features and it can move independently of bone structures. Therefore typical methods such as using landmarks to evaluate the accuracy of the registration are not applicable here.

We choose to contour the prostate in the mid-section for both the fixed and moving image before and after registration. The overlay of the two gives us an idea of how well the registration has performed (Figure 3). The overlay should capture the correctness not only in the axial plane but also in the superior and inferior direction, since a misalignment of more than one image slice would also cause misalignment in the visible axial plane. We paid more attention to the anterior side of the prostate contour since it is more visible.

### 2.4 Biopsy error and prostate movement calculations

**Biopsy needle placement error—**The biopsy *needle placement error* was determined by the distance from the original target position to the biopsy needle trajectory line (Figure 4). This distance is of how much the robot had missed the intended target. The clinician selects the original target in RAS coordinates (where the center of the prostate is

approximately the origin) from the pre-insertion volume. The needle trajectory line was obtained by using two needle tip coordinates from the post insertion volume.

**Target displacement—**The *target displacement* was calculated as the distance between the original and transformed target (Figure 4). The transformed target was obtained by applying the transformations from registration to the original target. To examine the relationship between needle insertion and prostate movement, the target displacement was decomposed into two components: one parallel to the needle vector, and the other orthogonal to it. The orthogonal component was then further broken down into motions in the left-right, anterior-posterior, and inferior-superior direction in order to analyze the prostate movement that was not parallel to the needle.

**Biopsy error—**The *biopsy error* was measured as the distance from the transformed target to the needle trajectory line (Figure 4). This is relevant for assessing accuracy since the tissue biopsy core is 1.5cm long. This number represents the distance between planned and actual biopsy location.

## 3. RESULTS

### 3.1 Registration accuracy

A total of 20 biopsies from 5 different patients were evaluated. Based on contour overlay, the registration error was less than 2 mm for patients who have moved less than 5 mm between the two image volumes. There was 1 patient who had movements larger than 10 mm. The large motion had caused a slight deformation of the prostate; therefore rigid registration could not capture the transformations completely. Three of his biopsies were excluded from the biopsy error analysis in this study.

### 3.2 Biopsy accuracy

The mean needle placement error, target displacement, and biopsy error was 2.2 mm (range: 0.5–5.7 mm), 5.4 mm (range: 1.6–11.1 mm), and 5.1 mm (range: 1.6–11 mm) respectively. Figure 5a shows the histograms of these numbers for all biopsy cases.

Target displacement parallel and orthogonal to the needle insertion direction was also calculated. The average motion parallel to the needle direction was only 1.4 mm, whereas the average orthogonal motion was 4.5 mm. For the orthogonal component, 82% of the biopsies showed a positive movement towards the superior direction. Figure 5b shows the axial, sagittal, and coronal view of the orthogonal component in RAS coordinates. Table 1 is a summary of all the results from the biopsy accuracy analysis.

## 4. DISCUSSION

The image slice thickness used in this study is 3 mm, and the diameter of a clinically significant tumor is between 2.5–5 mm. Since the average needle placement error (2.2 mm) is below both of these numbers, it can be considered as clinically acceptable. This confirms that the robot needle placement is accurate enough to hit the intended target. However, this measurement assumes that there was no prostate motion during the procedure. In reality, the prostate dislocates during the needle insertion, causing the target to move. Based on the cases studied, there was an average target displacement of 5.4 mm, which caused an average biopsy error of 5.1 mm.

By comparing the displacement components parallel and orthogonal to the needle insertion direction, it was found that the movement in the needle direction was not dominant. For the

orthogonal component, the positive movement towards the superior direction shown by 82% of the biopsies can be explained since the needle was pushing out of the rectum towards the prostate in a superior-anterior direction, therefore forcing the organ to move along.

## 5. CONCLUSION

In conclusion, based on the transverse prostate contour overlay, our rigid registration algorithm using mutual information can capture prostate motion during biopsy when the patient movement is less than 5 mm. We also found that the preplanned biopsy targets dislocated during the procedure and that the prostate motion is different from patient motion and the needle insertion direction. This suggests that methods such as real time prostate tracking can be used to improve the targeting accuracy of the biopsy procedure.

## 6. NOVELTY AND ORIGINALITY

We developed a registration algorithm to determine prostate motion during biopsy and used this information to evaluate the targeting accuracy of an MRI-guided robotic biopsy system from the U.S. National Cancer Institute. This work has not been submitted for publication or presentation elsewhere.

## Acknowledgments

We would like to thank the following physicians for their clinical data collection at the U.S. National Institutes of Health (NIH): Dr. Cynthia Menard, Dr. Anurag Singh, Dr. Jonathan A. Coleman, Dr. Robert L. Grubb, Dr. J.B Latouf, and Dr. Peter Pinto.

This research is supported by NIH 5R01CA111288-04 and 5R01EB002963-05.

## REFERENCES

1. Jemal A, Siegel R, Ward E, Hao Y, Xu J, Thun M. Cancer statistics, 2009. CA Cancer J Clin 2009;59(4):225–249. [PubMed: 19474385]
2. Krieger A, Susil R, Menard C, Coleman J, Fichtinger G, Atalar E, Whitcomb LL. Design of novel MRI compatible manipulator for image guided prostate interventions. IEEE Trans. on Biomed. Eng 2005;52(2):306–312.
3. Presti JC Jr. Prostate cancer: Assessment of risk using digital rectal examination, tumor grade, prostate-specific antigen, and systematic biopsy. Radiol. Clin. North Amer 2000;38(1):49–58. [PubMed: 10664666]
4. Terris MK, Wallen EM, Stamey TA. Comparison of mid-lobe versus lateral systematic sextant biopsies in detection of prostate cancer. Urol. Int 1997;59:239–242. [PubMed: 9444742]
5. Norberg M, Egevad L, Holmberg L, Sparen P, Norlen BJ, Busch C. The sextant protocol for ultrasound-guided core biopsies of the prostate underestimates the presence of cancer. Urology 1997;50(4):562–566. [PubMed: 9338732]
6. Rabbani F, Stroumbakis N, Kava BR, Cookson MS, Fair WR. Incidence and clinical significance of false-negative sextant prostate biopsies. J Urol 1998;159(4):1247–1250. [PubMed: 9507846]
7. Wefer AE, Hricak H, Vigneron DB, Coakley FV, Lu Y, Wefer J, Mueller-Lisse U, Carroll PR, Kurhanewicz J. Sextant localization of prostate cancer: comparison of sextant biopsy, magnetic resonance imaging and magnetic resonance spectroscopic imaging with step section histology. J Urol 2000;164(2):400–404. [PubMed: 10893595]
8. Susil RC, Ménard C, Krieger A, Coleman JA, Camphausen K, Choyke P, Fichtinger G, Whitcomb LL, Coleman CN, Atalar E. Transrectal prostate biopsy and fiducial marker placement in a standard 1.5T magnetic resonance imaging scanner. J Urol 2006;175(1):113–120. [PubMed: 16406885]

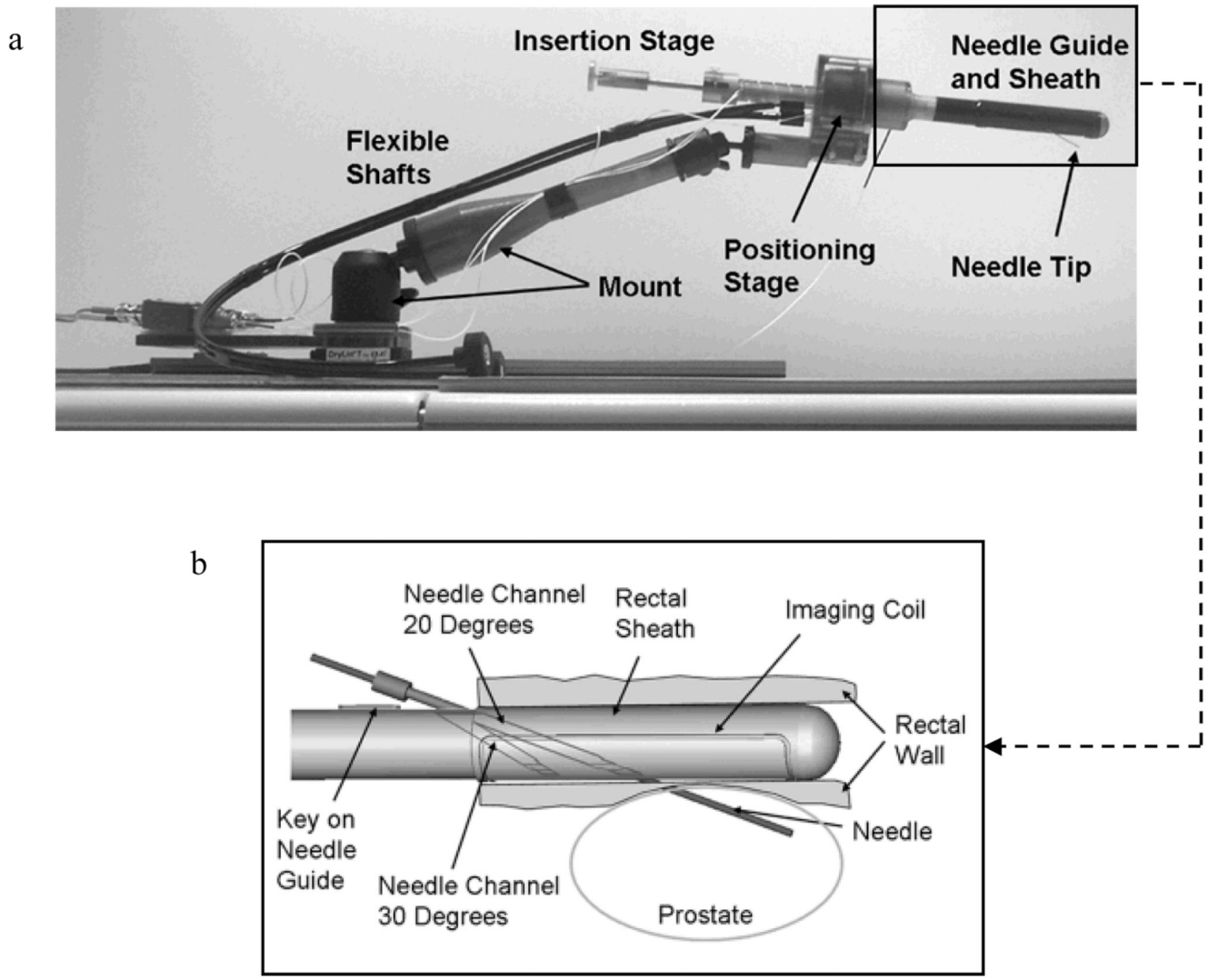


**Figure 1.**

a A picture of the MRI-guided robotic prostate biopsy system showing the different components.[2]

b The needle guide and sheath with straight needle channel used for biopsies analyzed in this paper.[2]

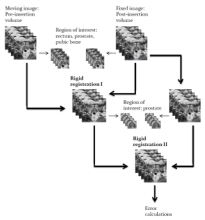


**Figure 2.**
The workflow of the two-step 3D–3D rigid registration using mutual information between pre and post needle insertion images. The region of interest for the first step includes the prostate, rectum, and pubic bone. The prostate was used as the region of interest in the second step.

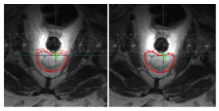

**Figure 3.**
Rigid registration validation by using 2D contour overlays of fixed and moving image before (left) and after (right) registration.

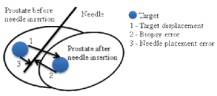


**Figure 4.**
A diagram illustrating the prostate motion during needle insertion and biopsy error calculations.

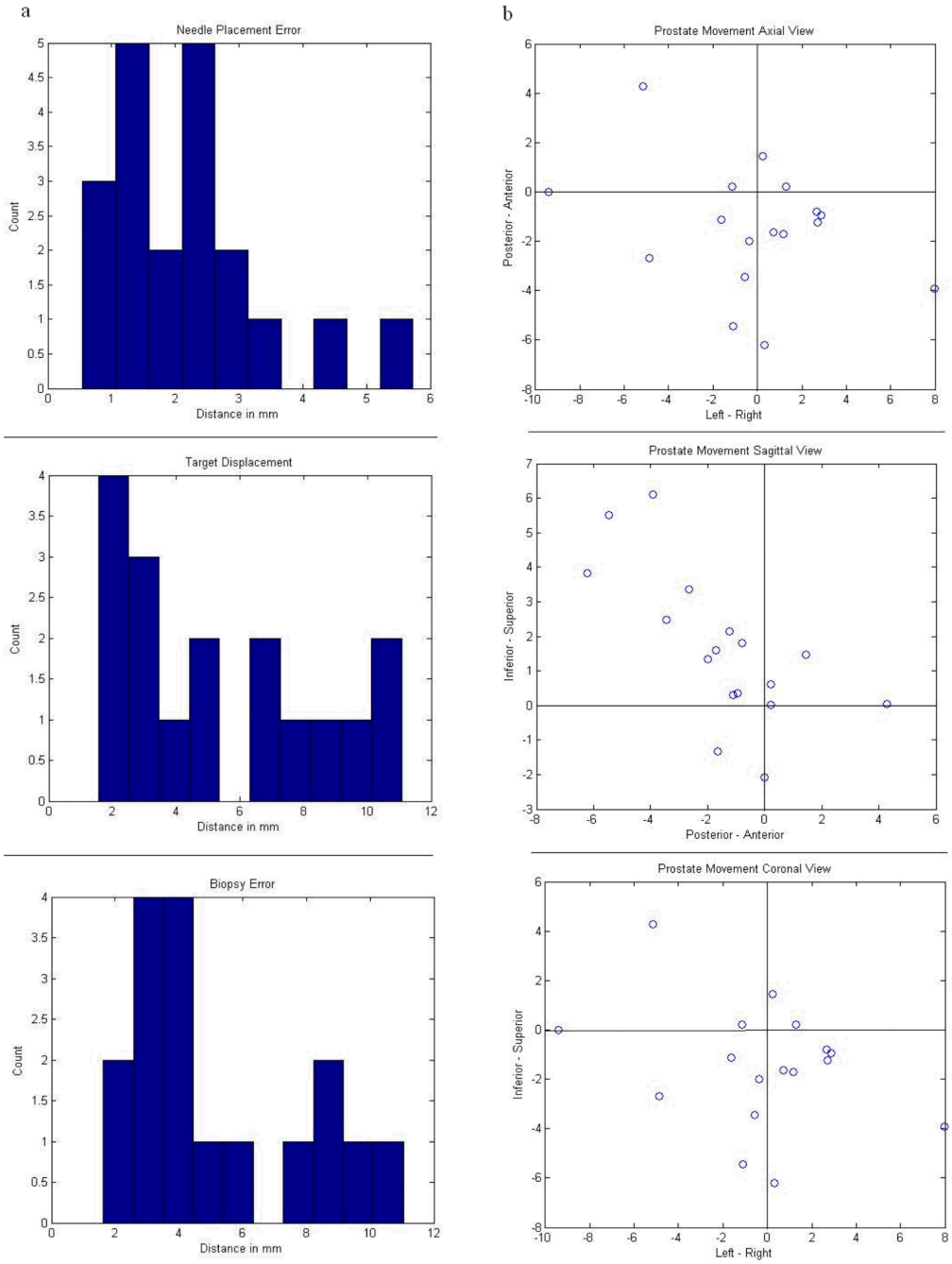


**Figure 5.**

a Histogram of needle placement errors (top), target displacements (middle), and biopsy errors (bottom).

b The axial (top), sagittal (middle), and coronal (bottom) view of the target displacement (mm) orthogonal to the needle insertion direction.

**Table 1**

Summary of results for biopsy accuracy validation.

| Patient | Biopsy Number | Target Displacement (mm) | Biopsy Error (mm) | Needle Placement Error (mm) | Target Displacement Parallel to Needle Direction (mm) | Target Displacement Orthogonal to Needle Direction (mm) | Orthogonal Component in RAS (mm) |
|---|---|---|---|---|---|---|---|
| A | 1 | NA | NA | 3.5 | NA | NA | NA |
| A | 2 | NA | NA | 0.5 | NA | NA | NA |
| A | 3 | NA | NA | 1.6 | NA | NA | NA |
| A | 4 | 1.6 | 2.8 | 2.5 | −0.6 | −1.5 | 1.3 0.2 0.6 |
| A | 5 | 4.3 | 1.6 | 4.3 | −3 | −3 | 2.9 −0.9 0.3 |
| A | 6 | 2.2 | 3 | 2.9 | −0.1 | −2.2 | 0.7 −1.6 −1.3 |
| B | 1 | 7 | 4.3 | 1.2 | 5.5 | −4.3 | −0.6 −3.4 2.5 |
| B | 2 | 9.9 | 8.5 | 0.8 | 6 | −7.8 | −1.1 −5.45 5.5 |
| B | 3 | 1.9 | 3 | 2.1 | 1.5 | −1.2 | −1.1 0.2 0 |
| C | 1 | 2.6 | 3.4 | 2.6 | 0 | −2.6 | 1.2 −1.7 1.6 |
| C | 2 | 10.8 | 11 | 1.4 | −1.1 | −10.8 | 8 −3.9 6.1 |
| C | 3 | 7.8 | 7.7 | 1.7 | 4.3 | −6.5 | −4.9 −2.7 3.4 |
| C | 4 | 9.1 | 8.5 | 1.2 | 5.4 | −7.3 | 0.3 −6.2 3.8 |
| D | 1 | 4.5 | 5.7 | 2.3 | −2.6 | −3.6 | 2.7 −1.2 2.1 |
| D | 2 | 3.3 | 4.3 | 5.7 | −0.3 | −3.3 | 2.7 −0.8 1.8 |
| D | 3 | 7 | 4.5 | 2.2 | −1.8 | −6.7 | −5.2 4.3 0.1 |
| D | 4 | 4.6 | 2 | 1.4 | 4.2 | −2.1 | 0.2 1.4 1.5 |
| E | 1 | 2.6 | 4.2 | 3.1 | 1.7 | −2 | −1.6 −1.1 0.3 |
| E | 2 | 2.4 | 4 | 1.8 | −0.3 | −2.4 | −0.4 −2 1.3 |
| E | 3 | 11.1 | 9.2 | 1.1 | 5.4 | −9.7 | −9.4 0 −2.1 |